Thermal expansion of gypsum investigated by neutron powder diffraction

PAUL F. SCHOFIELD,[1] KEVIN S. KNIGHT,[2] AND IONA C. STRETTON[3]

[1]Department of Mineralogy, Natural History Museum, Cromwell Road, London SW7 5BD, U.K.
[2]ISIS Science Division, Rutherford Appleton Laboratory, Chilton, Didcot OX11 0QX, U.K.
[3]Department of Earth Science, University of Manchester, Oxford Road, Manchester M13 9PL, U.K.

ABSTRACT

The cell parameters of deuterated gypsum have been extracted from Rietveld analysis of powder neutron diffraction data within the temperature range 4.2–320 K. The thermal expansion of gypsum is highly anisotropic along the b axis principally because of the effect of the D2$\cdots$O1 hydrogen bond. The high-temperature limits for the expansion coefficients for the cell edges a, b, and c are 3.98×10^{-6}, 4.36×10^{-5}, and 2.53×10^{-5} K^{-1}, respectively, and for the cell volume the limit is 6.96×10^{-5} K^{-1}. The β angle displays oscillatory variation, reflecting a change in the influence of at least two coupled processes. Empirical data analysis, within this temperature range, results in $\alpha_\beta = 1.251 \times 10^{-6} \sin(0.0116T + 0.311)$ K^{-1}.

INTRODUCTION

Gypsum is the most common sulfate mineral and is usually found within evaporite sequences or associated with calcareous sedimentary deposits. Large deposits of alabaster gypsum are commonly observed at the sole of many large-scale tectonic dislocations and thrust faults (Heard and Rubey 1966) within evaporitic regions. Hubbert and Rubey (1959) suggested that elevated pore pressures within such sequences reduce the overall normal stress across potential failure planes, greatly enhancing the probability of the formation of such large-scale overthrusts. It is likely that such abnormally high pore pressures are generated by the decomposition of hydrous mineral phases at depth, and consequently there have been many studies of the effect of dehydration and syntectonic metamorphic change on the deformation properties of certain materials (e.g., Rutter and Brodie 1988). To generate flow laws and to model the deformation properties of gypsum a full understanding of the temperature-dependent structural behavior is required.

The crystal structure of gypsum was first solved by Wooster (1936) using single-crystal X-ray diffraction. Bragg (1937) recalculated these data to transform the C cell, chosen by Wooster, to an I cell, and the resulting space group, $I2/a$, has been used in subsequent structural studies (Atoji and Rundle 1958; Cole and Lancucki 1974; Pedersen and Semmingsen 1982).

The thermal behavior of gypsum has been shown to be somewhat unique. For example, the optical properties of gypsum as a function of temperature, monitored by Hutchinson and Tutton (1913), change dramatically with the convergence of the refractive indices β and γ, on increasing temperature, and their crossing over at about 363 K. At this point the optic axial plane becomes perpendicular to (010), which is parallel to the optic axial plane below 363 K, necessitating structural or symmetry modifications in response to the temperature variations. The thermal dehydration reactions and products of gypsum have been extensively studied at both negligible vapor pressures (e.g., Lager et al. 1984; Putnis et al. 1990) and under various confining pressures (e.g., McConnell et al. 1987; Abriel et al. 1990), revealing a small stability field for gypsum, terminated by the onset of dehydration. The response of the gypsum structure to temperature variations does not appear to have been studied in detail by diffraction techniques, so we have used time-of-flight powder neutron diffraction to monitor the thermal behavior of gypsum within the temperature range 4.2–320 K.

EXPERIMENTAL METHODS

The material used for these experiments was Voltarre gypsum from Tuscany, Italy. Chemical analyses by ICP and anion chromatography showed that the only trace elements of any significance were Sr and Ce both at the 0.1 wt% level. Because of the large incoherent cross section for the scattering of thermal neutrons from protons, it was necessary to deuterate the sample for powder diffraction experiments to avoid large backgrounds and improve the signal-to-noise ratio. Deuteration of the gypsum, by simple rehydration of dehydrated gypsum using D_2O, was performed just prior to the experiment to minimize H $\leftrightarrow$ D exchange.

Neutron time-of-flight powder diffraction data were collected on the medium resolution diffractometer POLARIS (Smith et al. 1994) at the ISIS neutron spallation source, Rutherford Appleton Laboratory, U.K. (Wilson 1995). Just over 2 g of deuterated gypsum was packed into an indium-sealed cylindrical vanadium can with an internal diameter of 12 mm. The sample was quenched in liquid nitrogen before being placed in an ILL "Orange"
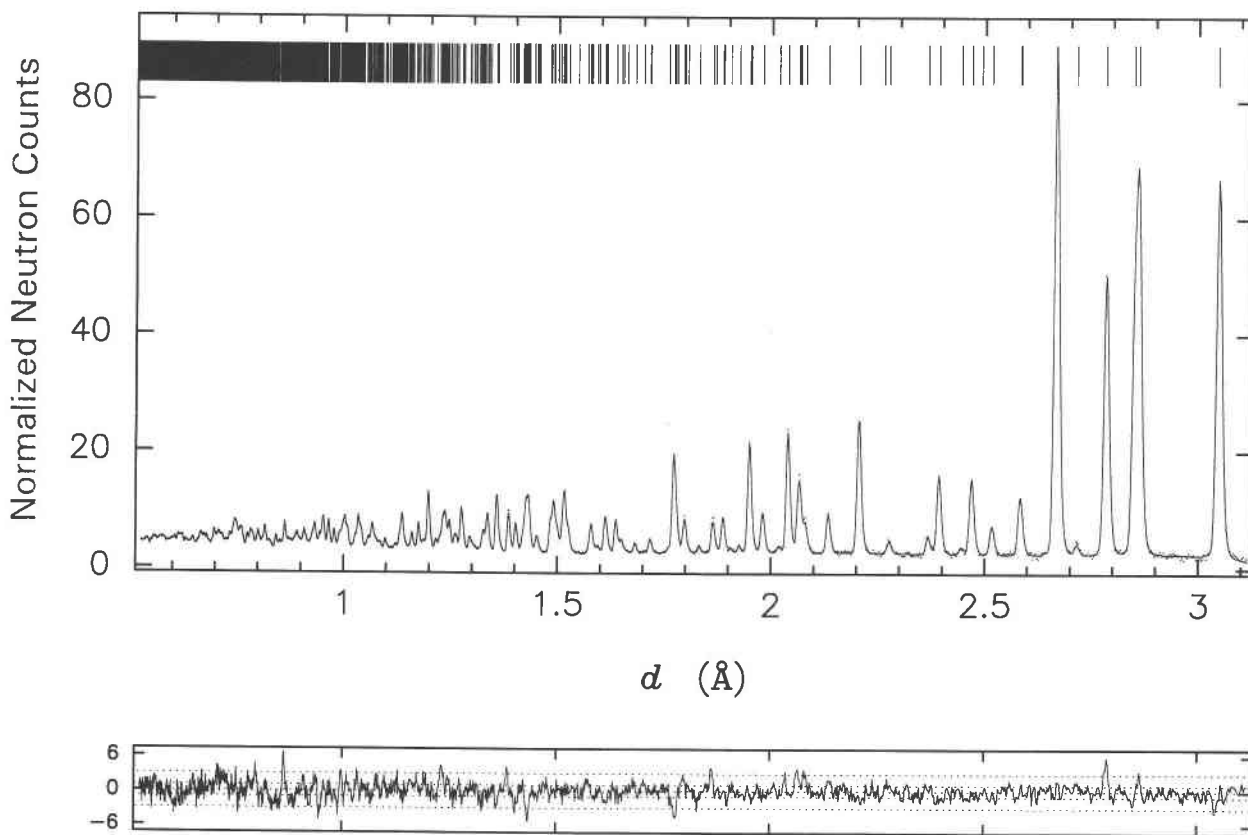
FIGURE 1. Neutron powder diffraction profile of gypsum at 4.2 K. The dots represent the observed data, and the solid line represents the calculated profile. The limits on the residual plot are ±3σ.

cryostat and cooled to 4.2 K. Diffraction patterns were collected for a total of 350 μA-h, initially at 4.2 K, then at 10 K, and subsequently at intervals of 10 K up to 320 K, with an equilibration time of 5 min. A series of four isothermal experiments were performed at 330 K as a check for the onset of dehydration.

Data in the time-of-flight range 3500–19250 μs in the backscattering detector bank ($2\theta = 145°$) were "binned" as $\Delta t/t = 0.001$, background subtracted, normalized to the incident flux distribution using the isotropic incoherent scattering from a vanadium rod, and were finally corrected for absorption and self scattering. These data were subsequently used in Rietveld profile refinement.

DATA REFINEMENT

The cell parameters used in the calculation of the thermal expansion were calculated during Rietveld profile refinements, which were performed using the dedicated time-of-flight package TF14LS (David et al. 1993) based on the Cambridge Crystallographic Subroutine Library. The first refinement was performed on the data collected at 4.2 K using the coherent scattering lengths from Sears (1992) (Ca 4.70, S 2.847, O 5.803, and D 6.671 fm), with the starting model based on the coordinates of Pedersen and Semmingsen (1982). The calculated parameters for

this refinement were then used as the initial data set for the subsequent refinement, in this case for the profile at 10 K, and so on for the remaining temperatures.

Figure 1 shows the final fit to the data for deuterated gypsum at 4.2 K, with the dots representing the diffraction data and the solid line showing the calculated profile. The difference between the diffraction profiles divided by the estimated standard deviation is shown with the horizontal dotted lines reflecting ±3σ, and agreement factors $R_p = 2.84$, $R_{wp} = 2.25$, and $R_{exp} = 1.49\%$ are for 1779 observations and 41 variables. The large incoherent scattering of neutrons caused by H can be used to assess the degree of deuteration of the gypsum used in this study. The low background intensity indicates that the deuteration of the gypsum was very high, and attempts to refine the data by incorporating protons within the model indicated that the D content was above 99% of the expected total.

LATTICE EXPANSION

The lattice parameters, extracted from the Rietveld analyses, for gypsum within the temperature range 4.2–320 K are given in Table 1 and displayed in Figure 2. These data show that the thermal expansion of gypsum is extremely anisotropic, with the b lattice parameter in-
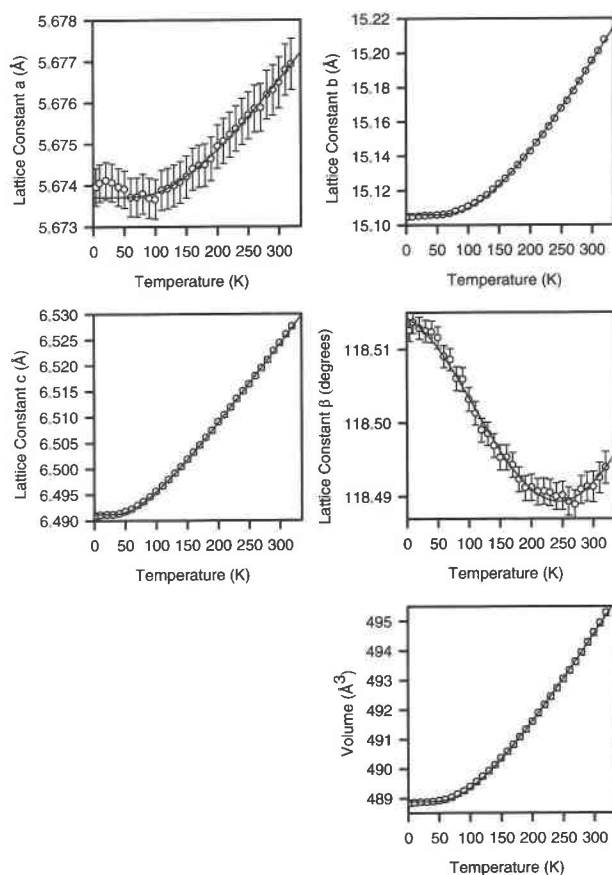
TABLE 1. The lattice parameters of deuterated gypsum from 4.2 to 320 K

T (K)	a (Å)	b (Å)	c (Å)	β (°)	V (Å³)
4.2	5.6740(5)	15.1049(2)	6.4909(4)	118.513(2)	488.83(8)
10	5.6741(5)	15.1049(2)	6.4910(4)	118.514(2)	488.84(8)
20	5.6741(5)	15.1053(2)	6.4911(4)	118.513(2)	488.87(8)
30	5.6741(5)	15.1054(2)	6.4911(4)	118.513(2)	488.87(8)
40	5.6740(5)	15.1056(2)	6.4914(4)	118.512(2)	488.88(8)
50	5.6739(5)	15.1058(2)	6.4917(4)	118.512(2)	488.92(8)
60	5.6737(5)	15.1060(2)	6.4922(4)	118.510(2)	488.96(8)
70	5.6737(5)	15.1065(2)	6.4929(4)	118.510(2)	489.03(8)
80	5.6738(5)	15.1079(2)	6.4936(4)	118.510(2)	489.15(8)
90	5.6737(5)	15.1091(2)	6.4946(4)	118.510(2)	489.25(8)
100	5.6737(5)	15.1108(2)	6.4956(4)	118.503(2)	489.39(8)
110	5.6739(5)	15.1126(2)	6.4966(4)	118.501(2)	489.55(8)
120	5.6739(5)	15.1151(2)	6.4979(4)	118.499(2)	489.74(8)
130	5.6740(5)	15.1174(2)	6.4991(4)	118.499(2)	489.92(9)
140	5.6741(5)	15.1205(2)	6.5004(4)	118.497(2)	490.13(9)
150	5.6742(5)	15.1236(2)	6.5018(4)	118.495(2)	490.36(9)
160	5.6744(5)	15.1268(2)	6.5032(4)	118.495(2)	490.58(9)
170	5.6745(5)	15.1305(2)	6.5046(4)	118.494(2)	490.82(9)
180	5.6745(5)	15.1347(2)	6.5061(4)	118.492(2)	491.08(9)
190	5.6746(5)	15.1388(2)	6.5074(4)	118.491(2)	491.33(9)
200	5.6749(5)	15.1427(2)	6.5091(4)	118.491(2)	491.60(9)
210	5.6751(6)	15.1478(2)	6.5104(4)	118.491(2)	491.89(9)
220	5.6752(6)	15.1524(2)	6.5119(4)	118.491(2)	492.16(9)
230	5.6754(6)	15.1571(2)	6.5135(4)	118.491(2)	492.45(9)
240	5.6755(6)	15.1618(2)	6.5150(4)	118.490(2)	492.73(9)
250	5.6757(6)	15.1677(2)	6.5164(4)	118.490(2)	493.04(9)
260	5.6759(6)	15.1722(2)	6.5180(5)	118.489(2)	493.3(1)
270	5.6759(6)	15.1777(2)	6.5195(5)	118.489(2)	493.6(1)
280	5.6762(6)	15.1833(2)	6.5211(5)	118.491(2)	493.9(1)
290	5.6763(6)	15.1893(2)	6.5228(5)	118.491(2)	494.3(1)
300	5.6765(6)	15.1952(3)	6.5243(5)	118.491(2)	494.6(1)
310	5.6768(6)	15.2008(3)	6.5260(5)	118.493(2)	494.9(1)
320	5.6769(6)	15.2074(3)	6.5277(5)	118.494(2)	495.3(1)

FIGURE 2. Variation of the lattice parameters of gypsum within the temperature range 4.2–320 K. The raw data are shown with the calculated fits employing Einstein functions for all parameters except the β angle, which was empirically fitted by a cosine function.

creasing by 0.1025 Å and the a and c lattice parameters increasing by 0.0029 and 0.0368 Å, respectively. The increase in the volume is 6.47 Å³, which represents some 1.3% of the volume at 4.2 K and principally reflects the anisotropy along the b axis.

On increasing temperature the a cell parameter indicates an apparent negative thermal expansion below 90 K, whereas above 90 K it increases more regularly as a function of temperature. This cannot, however, be fully clarified at this stage and may simply result from the small total expansion along a and the subsequent proportionally large error. Both the b and c cell parameters vary more regularly, with little initial response followed by a near-linear increase as a function of increasing temperature. Note that the onset of significant expansion does not occur at the same temperature for these cell edges, with a, b, and c showing minimal or no increases below about 100, 80, and 50 K, respectively.

The β angle also displays an unusual variation as a function of increasing temperature, which is oscillatory over the temperature range investigated, yet the maximum variation is only 0.024°. With minimal variation below about 40 K, the β angle decreases almost linearly until about 200 K, where it remains fairly constant before showing a rapid increase above about 270 K. These anomalous behaviors in both the a cell parameter and

the β angle are not evident in the volume expansion, which appears to vary in the expected manner and is dominated by the large anisotropy along the b axis.

All the unit-cell parameters are well fitted to an Einstein expression of the form $X = X_0 + K/(e^{\vartheta/T} - 1)$, where X_0 is the parameter X at 0 K, K is the Einstein constant, T is the temperature in kelvins between 4.2 and 330, and ϑ is the effective Einstein temperature. Because the β cell angle showed oscillatory behavior it was fitted empirically with a general cosine function of the form $\beta = \beta' + A \cos(\omega T + \phi)$, oscillating around β' with amplitude A, effective angular frequency ω, and phase shift ϕ. Because of the uncertainty of the trend shown by the a lattice parameter below 50 K these data were excluded from the fitting procedure. These fits and the raw data are displayed graphically in Figure 2 and are tabulated with the associated errors derived from the fitting process in Table 2.

The instantaneous (isobaric) thermal expansion is related to the unit-cell parameter x, where $\alpha_x = (1/x_0)(\delta x/\delta T)$ and x_0 is the magnitude of parameter x at 0 K. At high temperatures $e^{\vartheta/T} \approx 1 + (\vartheta/T)$, using a Taylor's ex-

TABLE 2. Tabulated results and errors from the data-fitting procedures

	X_0	K	ϑ (K)
a	5.67371(4) Å	0.010(1)	461(24)
b	15.1059(2) Å	0.282(7)	428(5)
c	6.4911(4) Å	0.0370(5)	225(2)
V	488.89(1) Å³	11.0(2)	322(4)

Note: X_0, K, and ϑ represent the 0 K cell-parameter value, the Einstein constant, and the effective Einstein temperatures, respectively. The data from the empirical cosine fit to the β-angle variation reflect oscillation about β' [118.5021(4)], amplitude A [0.0128(4)], effective angular frequency ω [0.0116(4)], and phase shift ϕ [0.310(95)].

TABLE 3. Atomic coordinates and isotropic displacement factors for deuterated gypsum at 4.2, 150, and 320 K

	x	y	z	B (Å²)
4.2 K*				
Ca	0.50	0.07996(18)	0.25	0.098(25)
S	0.00	0.07667(24)	0.75	0.104(43)
O1	0.96413(26)	0.13282(8)	0.55028(23)	0.297(18)
O2	0.75763(27)	0.02194(9)	0.66427(22)	0.280(20)
Ow	0.38342(29)	0.18240(10)	0.46179(24)	0.318(18)
D1	0.25369(30)	0.16662(9)	0.50769(28)	1.428(22)
D2	0.40549(33)	0.24481(10)	0.49322(28)	1.288(25)
150 K				
Ca	0.50	0.07984(21)	0.25	0.207(32)
S	0.00	0.07695(29)	0.75	0.237(56)
O1	0.96371(33)	0.13292(10)	0.55070(29)	0.602(25)
O2	0.75753(33)	0.02170(12)	0.66443(27)	0.518(26)
Ow	0.38222(38)	0.18229(13)	0.46024(33)	0.795(26)
D1	0.25341(41)	0.16210(12)	0.50655(36)	1.911(31)
D2	0.40493(42)	0.24446(12)	0.49252(36)	1.728(34)
320 K				
Ca	0.5	0.07864(32)	0.25	0.570(57)
S	0.0	0.07872(42)	0.75	0.504(50)
O1	0.96164(50)	0.13263(15)	0.55120(43)	1.177(43)
O2	0.75714(48)	0.02154(18)	0.66527(39)	0.970(41)
Ow	0.37837(60)	0.18255(21)	0.46544(54)	1.749(49)
D1	0.25043(64)	0.16150(20)	0.50086(61)	3.520(66)
D2	0.40225(69)	0.24347(20)	0.49003(61)	3.074(66)

Note: At 4.2 K, R_p = 2.84, R_{wp} = 2.25, and R_{exp} = 1.49%; at 150 K, R_p = 2.60, R_{wp} = 2.09, and R_{exp} = 1.34%; and at 320 K, R_p = 2.66, R_{wp} = 2.19, and R_{exp} = 1.30%.
* Refer to David et al. (1993) for definition of discrepancy indices.

pansion, and consequently $(1/x_0)(\delta x/\delta T) \approx K/(x_0\vartheta)\cdot[1 + (\vartheta/T)]$, giving, for the cell parameters

$$\alpha_a = \left(\frac{1}{a_0}\right)\left(\frac{\delta a}{\delta T}\right) \approx \frac{K}{(a_0\vartheta)}\cdot\left[1 + \left(\frac{\vartheta}{T}\right)\right]$$
$$= 3.98 \times 10^{-6}\left[1 + \left(\frac{\vartheta}{T}\right)\right] \quad (1)$$

$$\alpha_b = \left(\frac{1}{b_0}\right)\left(\frac{\delta b}{\delta T}\right) \approx \frac{K}{(b_0\vartheta)}\cdot\left[1 + \left(\frac{\vartheta}{T}\right)\right]$$
$$= 4.36 \times 10^{-5}\left[1 + \left(\frac{\vartheta}{T}\right)\right] \quad (2)$$

$$\alpha_c = \left(\frac{1}{c_0}\right)\left(\frac{\delta c}{\delta T}\right) \approx \frac{K}{(c_0\vartheta)}\cdot\left[1 + \left(\frac{\vartheta}{T}\right)\right]$$
$$= 2.53 \times 10^{-5}\left[1 + \left(\frac{\vartheta}{T}\right)\right] \quad (3)$$

$$\alpha_V = \left(\frac{1}{V_0}\right)\left(\frac{\delta V}{\delta T}\right) \approx \frac{K}{(V_0\vartheta)}\cdot\left[1 + \left(\frac{\vartheta}{T}\right)\right]$$
$$= 6.96 \times 10^{-5}\left[1 + \left(\frac{\vartheta}{T}\right)\right] \quad (4)$$

and the instantaneous thermal expansion for the β cell angle is

$$\alpha_\beta = (1/\beta_0)(\delta\beta/\delta T) = -(A\omega/\beta_0)\sin(\omega T + \phi)$$
$$= 1.251 \times 10^{-6}\sin(0.0116T + 0.311) \quad (5)$$

reflecting the change in sign of the thermal expansion.

The influence of the temperature on the thermal expansion can be seen from Equations 1 to 5. For a, b, c, and V the rate of decrease of the thermal expansion coefficient decreases as the temperature increases, leading to high-temperature limits of 3.98×10^{-6}, 4.36×10^{-5}, 2.53×10^{-5}, and 6.96×10^{-5} K^{-1}, respectively.

Gypsum can be considered to be a layered structure, with layers parallel to the (010) face. Two sheets comprising SO_4^{2-} units are bound together by CaO_8 polyhedra, with six O atoms shared with the SO_4^{2-} groups and two O atoms with H_2O molecules. These pairs of layers are weakly bound together by a layer of H_2O molecules, which

explains the perfect {010} cleavage. Seidl et al. (1969) showed that although the H_2O molecules are equivalent, they are significantly distorted in comparison to the geometry of free H_2O molecules. The H-O-H bond angle of these H_2O molecules is 107.5°, the two nonequivalent H-O bonds are 0.959 and 0.942 Å, and although the longest O-H···O hydrogen bond approximates linearity with an angle of 177.2°, the shortest hydrogen bond possesses an angle of 170.9° (Pedersen and Semmingsen 1982). Atomic coordinates, isotropic displacement factors, bond lengths, and bond angles extracted from the Rietveld analysis for the temperatures 4.2, 150, and 320 K are shown in Tables 3 and 4.

From the structure it can be seen that the response of the D_2O molecules to temperature increases depicts the behavior of the thermal expansion of gypsum. Indeed, the hydrogen bond D2···O1 acts almost totally along b, binding the layers together, and the thermal response of this weak interaction amounts to an increase of 0.039 Å, resulting in a total D2···O1 effect of 0.078 Å per unit cell. This reflects about 75% of the expansion along b and when coupled with the expansion of the polyhedral layers, with a large component of the Ca-Ow bond along b, is the principal cause of the large expansion along this axis. Further expansion along the b axis may be hindered by the inability of the D-O-D angle of the D_2O molecule to further distort and the compensatory decrease of the Ow-D2 bond.

TABLE 4. Selected bond lengths (Å) and angles (°) for deuterated gypsum at 4.2, 150, and 320 K

	4.2 K	150 K	320 K
Ca-O1	2.544(1)	2.546(2)	2.548(3)
Ca-O2	2.526(2)	2.532(3)	2.541(3)
Ca-O2′	2.365(2)	2.362(3)	2.351(4)
Ca-Ow	2.364(3)	2.364(3)	2.378(5)
S-O1	1.480(3)	1.478(3)	1.461(5)
S-O2	1.468(2)	1.473(3)	1.495(5)
O1-S-O1′	110.0(2)	110.1(3)	111.7(4)
O2-S-O2′	111.4(2)	110.9(3)	108.9(4)
Ow-D1	0.966(3)	0.963(4)	0.961(6)
Ow-D2	0.960(2)	0.959(3)	0.948(4)
D1-Ow-D2	106.6(2)	106.6(3)	107.2(5)
D1-O1	1.846(3)	1.852(3)	1.872(5)
D2-O1	1.883(2)	1.890(2)	1.922(4)

The hydrogen bond D1···O1 has a large component along the a axis; however, the expansion along a is smaller than that along b or c. It is also evident from Table 4 that the expansion of the D1···O1 hydrogen bond (0.026 Å) is small in comparison with that of the D2···O1 hydrogen bond (0.039 Å) because the expansion of D1···O1 is also controlled by the thermal response of the strongly defined polyhedral layers of gypsum. The thermal expansion along a is likely to be hindered because of a combination of factors, including, for example, the decrease of the x fractional coordinate for all the nonsymmetry-restricted atoms, the inability of the D_2O molecule to increase the D1-Ow-D2 angle, the decrease in both the Ca-O2′ bond and the O2-S-O2′ angle, and the almost negligible expansion of the Ca-O1 bond.

As noted above, the β angle is relatively insensitive to variations in temperature, ranging several hundred kelvin in this study. The change in sign of the thermal expansion, however, suggests the involvement of two separate causative mechanisms. Initially β begins to decrease, perhaps reflecting a complex response to the combined variation of the atomic coordinates and not the result of a single dominant factor. Alternatively, this decrease may be induced by decreases in the Ca-O2′ bond and the O2-S-O2′ angle, whereas other bond lengths and angles remain fairly constant. At about 200 K, however, the β angle stops decreasing and remains constant for about 70° before rapidly increasing. At this point other structural parameters begin to dominate the thermal behavior of β; for example, the increase in the hydrogen bond D1···O1 or the Ca-Ow bond, both of which act partially across the β angle, or alternatively the increase in the O1-S-O1′ bond angle. Again, it is likely that the increase in the β angle is a combination of all of these factors; however, it does represent the convergence of the structural units toward an arrangement suitable for dehydration and subsequent transformation to disordered bassanite and finally hexagonal γ-CaSO$_4$, where the unique b axis of gypsum becomes the hexad-containing c axis of γ-CaSO$_4$ and the 118.513° β angle of gypsum becomes the 120° angle of γ-CaSO$_4$.

The thermal relaxation of the gypsum structure, as reported here, when coupled with compressibility data allows the generation of realistic flow laws for gypsum and in turn enhances the understanding of both static and dynamic deformation processes of gypsum. The thermal behavior of gypsum prior to dehydration enables the modeling of stresses associated with polycrystalline aggregates within fault zones and deformation regimes.

REFERENCES CITED

Abriel, W., Reisdorf, K., and Pannetier, J. (1990) Dehydration reactions of gypsum: A neutron and X-ray diffraction study. Journal of Solid State Chemistry, 85, 23–30.

Atoji, M., and Rundle, R.E. (1958) Neutron diffraction study of gypsum, CaSO$_4$·2H$_2$O. Journal of Chemical Physics, 29, 1306–1311.

Bragg, W.L. (1937) Atomic structure of minerals, 292 p. Cornell University Press, Ithaca, New York.

Cole, W.F., and Lancucki, C.J. (1974) A refinement of the crystal structure of gypsum CaSO$_4$·2H$_2$O. Acta Crystallographica, B30, 921–929.

David, W.I.F., Ibberson, R.M., and Matthewman, J.C. (1993) Powder diffraction at ISIS. Rutherford Appleton Laboratory Report no. RAL-92–032.

Heard, H.C., and Rubey, W.W. (1966) Tectonic implications of gypsum dehydration. Geological Society of America, 77, 741–760.

Hubbert, M.K., and Rubey, W.W. (1959) Role of fluid pressure in the mechanics of overthrust faulting. I. Bulletin of the Geological Society of America, 70, 115–166.

Hutchinson, A., and Tutton, A.E.H. (1913) Uber die Temperatur der optischen Einaxigkeit von Gyps. Zeitschrift für Kristallographie, 52, 218–224.

Lager, G.A., Armbruster, T., Rotella, F.J., Jorgensen, J.D., and Hinks, D.G. (1984) A crystallographic study of the low-temperature dehydration products of gypsum, CaSO$_4$·2H$_2$O, hemihydrate CaSO$_4$·0.5H$_2$O, and γ-CaSO$_4$. American Mineralogist, 69, 910–918.

McConnell, J.D.C., Astill, D.M., and Hall, P.L. (1987) The pressure dependence of the dehydration of gypsum to bassanite. Mineralogical Magazine, 51, 453–457.

Pedersen, B.F., and Semmingsen, D. (1982) Neutron diffraction refinement of the structure of gypsum, CaSO$_4$·2H$_2$O. Acta Crystallographica, B38, 1074–1077.

Putnis, A., Winkler, B., and Fernandez-Diaz, L. (1990) In situ IR spectroscopic and thermogravimetric study of the dehydration of gypsum. Mineralogical Magazine, 54, 123–128.

Rutter, E.H., and Brodie, K.H. (1988) Experimental "syn-tectonic" dehydration of serpentine under conditions of controlled pore water pressure. Journal of Geophysical Research, 93, 4907–4932.

Sears, V.F. (1992) Neutron scattering lengths and cross sections. Neutron News, 3, 26–37.

Seidl, V., Knop, O., and Falk, M. (1969) Infrared studies of water in crystalline hydrates: Gypsum, CaSO$_4$·2H$_2$O. Canadian Journal of Chemistry, 47, 1361–1368.

Smith, R.I., Hull, S., and Armstrong, A.R. (1994) The polaris powder diffractometer at ISIS. Material Science Forum, 166–169, 251–256.

Wilson, C.C. (1995) A guided tour of ISIS: The UK neutron spallation source. Neutron News, 6, 27–34.

Wooster, W.A. (1936) On the crystal structure of gypsum, CaSO$_4$·2H$_2$O. Zeitschrift für Kristallographie, 94, 375–396.